

RESEARCH ARTICLE | NOVEMBER 22 2023

# Spontaneous pattern of orthogonal ferroelectric domains in epitaxial KNN films

C. Groppi ; F. Maspero ; M. Asa ; G. Pavese ; C. Rinaldi ; E. Albisetti ; M. Badillo-Avila  ; R. Bertacco 



*J. Appl. Phys.* 134, 204102 (2023)

<https://doi.org/10.1063/5.0171349>

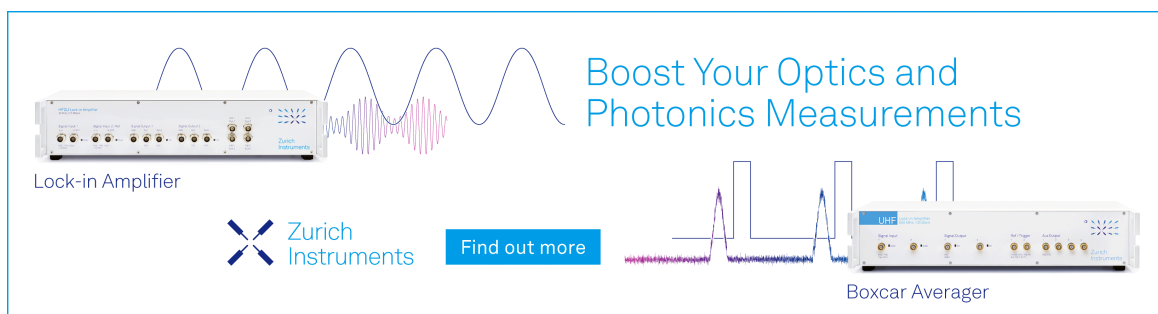


View Online



Export Citation

29 April 2024 13:07:06



Boost Your Optics and Photonics Measurements

Lock-in Amplifier

Zurich Instruments

Find out more

Boxcar Averager

# Spontaneous pattern of orthogonal ferroelectric domains in epitaxial KNN films

Cite as: J. Appl. Phys. 134, 204102 (2023); doi: 10.1063/5.0171349

Submitted: 8 August 2023 · Accepted: 5 November 2023 ·

Published Online: 22 November 2023



C. Groppi,<sup>1</sup>  F. Maspero,<sup>1,2</sup>  M. Asa,<sup>3</sup>  G. Pavese,<sup>1</sup>  C. Rinaldi,<sup>1</sup>  E. Albisetti,<sup>1</sup>  M. Badillo-Avila,<sup>1,a)</sup>   
and R. Bertacco<sup>1,3</sup> 

## AFFILIATIONS

<sup>1</sup>Department of Physics, Politecnico di Milano, Piazza Leonardo da Vinci 32, Milano 20133, Italy

<sup>2</sup>CNR Istituto di Fotonica e Nanotecnologie, Milano, Italy

<sup>3</sup>Polifab, Politecnico di Milano, Via Giuseppe Colombo 81, Milano 20133, Italy

<sup>a)</sup>Author to whom correspondence should be addressed: [miguelangel.badillo@polimi.it](mailto:miguelangel.badillo@polimi.it)

## ABSTRACT

Lead-free piezoelectric (K, Na)NbO<sub>3</sub> (KNN) is considered one of the promising candidates for the replacement of Pb(Zr<sub>x</sub>Ti<sub>1-x</sub>)O<sub>3</sub>. Several studies underlined the issue of K and Na volatility with increasing deposition temperatures, leading to high leakage currents in thin films, which still represents a major drawback for applications. This paper shows how epitaxial growth with concomitant preferred orientation of KNN films on niobium-doped strontium titanate (Nb:STO) depends on growth temperature and substrate strain. A preferred out-of-plane polar (001) orientation of KNN is obtained at high temperatures (>600 °C), while (100) orientation is dominant for lower ones. The (001) orientation is forced out-of-plane due to the sizeable in-plane stress derived from a negative lattice mismatch of pseudo-cubic KNN with respect to the underlying cubic (001) Nb:STO substrate. Moreover, we show that K-Na deficiency and high leakage of epitaxial KNN films deposited at high temperatures are accompanied by the appearance of a pattern of orthogonal spontaneous ferroelectric domains aligned to the [100] and [010] directions of Nb:STO. This pattern, visible in secondary electron microscopy, piezoforce response microscopy, and conductive atomic force microscopy images, is uncorrelated to the surface morphology. Supported by reciprocal space mapping by x-ray diffraction, this phenomenon is interpreted as the result of strain relaxation via ferroelectric domain formation related to K-Na deficient films displaying a sizable and increasing compressive strain when grown on Nb:SrTiO<sub>3</sub>. Our findings suggest that strain engineering strategies in thin films could be used to stabilize specific configurations of piezo- and ferroelectric domains.

© 2023 Author(s). All article content, except where otherwise noted, is licensed under a Creative Commons Attribution (CC BY) license (<http://creativecommons.org/licenses/by/4.0/>). <https://doi.org/10.1063/5.0171349>

## I. INTRODUCTION

Piezoelectric materials with high performances for an effective interconversion of mechanical and electrical energies have become a primary component for the development of technological elements such as actuators, transducers, and sensors in a variety of fields ranging from the automotive industry to medical diagnostics to telecommunications.<sup>1,2</sup>

In the past few years, (K<sub>x</sub>Na<sub>1-x</sub>)NbO<sub>3</sub> (KNN) has been the focus of vigorous research as a promising lead-free piezoelectric material with a perovskite structure,<sup>3,4</sup> thanks to its remarkable properties ( $d_{33}$  up to 416 pm/V in bulk KNN doped with Li, Ta, and Sb)<sup>5</sup> and high Curie temperature (around 400 °C).<sup>4</sup> Despite the excellent results well consolidated in the bulk ceramic material,<sup>3</sup> thin films of KNN are usually less performant and present

additional issues to be addressed.<sup>6</sup> The first issue is the high temperatures (500–700 °C) required to stabilize ferroelectric KNN films with orthorhombic and tetragonal crystalline phases,<sup>7–9</sup> which represents an evident obstacle to integration with CMOS electronics, typically requiring process temperatures below 450 °C. The second issue of KNN is the volatility of alkali elements<sup>9,10</sup> during growth or annealing processes, which in thin films results in severe current leakage.<sup>11</sup> Nevertheless, in the last years, efforts of the community working on lead-free piezoelectrics have led to significant advancements toward the exploitation of KNN. Some works demonstrated the possibility of synthesizing highly oriented KNN thin films on Pt/Ti/SiO<sub>2</sub>/Si by physical vapor deposition (PVD) processes such as sputtering or pulsed laser deposition (PLD) and chemical solution deposition (CSD) in favor of technological and industrial

29 April 2024 13:07:06

applications of silicon-based processes, such as in miniaturized devices in microelectromechanical systems (MEMS).<sup>7,8,12–15</sup> At variance, epitaxial KNN films grown onto perovskite substrates represent an exciting playground for the investigation of intrinsic phenomena in single-crystal heterostructures, avoiding interference of extrinsic causes related to grain boundaries, film texturation, and defects typical of polycrystalline films on Pt-terminated templates. The structure of epitaxial thin films, very close to that of single crystals with a preferential orientation, makes them ideal case studies for examining the mechanism of high piezoelectricity at the phase boundaries. Such studies acquire even more importance in light of the complicated phase diagram of KNN with respect to its well-known lead-containing analog PZT.<sup>16</sup> Some works, for instance, indicate that a sizable loss of Na and K suffered during film deposition is responsible for creating A-vacancies in the perovskite structure, which are mainly responsible for large leakage currents.<sup>17,18</sup>

In this paper, an investigation of the electrical and piezoelectric properties of epitaxial KNN thin films grown at various temperatures on (001)-oriented Nb:SrTiO<sub>3</sub> single-crystal substrates is discussed. A two-dimensional-like (2D) growth is observed at high temperatures (>600 °C). It is accompanied by a sizable increase in the leakage current due to the loss of Na and K during film deposition at high temperatures. The flatter 2D-like films are piezoelectric, although their mechanical response ( $d_{33}$  coefficient) is reduced compared to that of polycrystalline films,<sup>15</sup> as seen by piezoresponse force microscopy (PFM). Additionally, the emergence in 2D-like thin films of a configuration of spontaneous vertical and horizontal (thus, orthogonal to each other) domain patterns in films grown at 660 °C can be observed by PFM, conductive atomic force microscopy (C-AFM), and scanning electron microscopy (SEM) signals. This phenomenon is ascribed to a mechanism of relief of internal lattice stresses via the formation of ferroelectric domain walls along crystallographic axes, which occurs in addition to typical misfit dislocations.<sup>19,20</sup>

## II. METHODS

### A. Thin film growth

KNN thin films were deposited on single-crystal Nb:SrTiO<sub>3</sub> (Nb:STO) substrates with (001) orientation and a 0.5 wt. Nb-doping. KNN was grown by pulsed laser deposition. The PLD system exploits a Nd:YAG laser operating at its fourth harmonic wavelength of 266 nm. Substrates were cleaned with a treatment process that included an *ex situ* oxygen plasma (10 min) and an *in situ* annealing at 700 °C in an oxygen atmosphere (220 mTorr).<sup>15</sup> The optimized growth conditions comprise the following deposition parameters: an oxygen pressure of 220 mTorr, a substrate–target distance of 40 mm, and laser fluence of 1.3 J/cm<sup>2</sup> at 10 Hz. Different samples were grown varying the substrate temperature in the 470–740 °C range. Just after growth, an *in situ* 30-min annealing in 380 Torr of oxygen pressure was carried out at a temperature of 500 °C. The KNN sample thin films have a thickness of around 300 nm, except the sample grown at 740 °C (400 nm) due to an increased growth rate and three-dimensional aspect of the film at this high temperature.

### B. Structural and chemical characterization

*In situ* reflection high energy electron diffraction (RHEED) was used to evaluate the in-plane orientation of epitaxial films. The morphological properties of thin films were examined using a scanning electron microscope (Zeiss LEO 1525 FE-SEM operated at 10 kV). A dedicated module of the SEM was used to perform energy dispersive x-ray spectroscopy (EDS and EDX) to analyze the chemical composition of the samples under a probing electron beam with an energy of 10 keV.  $\theta$ – $2\theta$  x-ray diffraction (XRD) in out-of-plane and in-plane geometry, as well as reciprocal space maps (RSM) for the evaluation of lattice parameters, were acquired *ex situ* with an x-ray diffractometer, Rigaku SmartLab X (with a wavelength of 1.5406 Å).

### C. Electrical measurements

Electrical tests were performed on a matrix of Ti electrode capacitors of size  $38 \times 38 \mu\text{m}^2$  created by e-beam evaporation on top of the KNN films through a physical mask. Leakage current measurements were performed with a source meter (Keithley 2612) in the top-top configuration by supplying a triangular-like waveform of  $0 \rightarrow +210 \text{ kV/cm} \rightarrow 0 \rightarrow -210 \text{ kV/cm} \rightarrow 0$ , with a slope of 2.1 V/s.

### D. Piezoelectric characterization

Piezoelectric measurements and extraction of the  $d_{33}$  piezoelectric coefficient were carried out by piezoresponse force microscopy using a Keysight 5600LS atomic force microscope. Applying a small AC voltage of 2 V to the tip at a frequency (30 kHz) much lower than the contact resonance ( $\sim 330 \text{ kHz}$ ) made it possible to map spontaneous ferroelectric domains and estimate the piezoelectric coefficient. Piezoelectric hysteresis loops were recorded by progressively applying a DC voltage across the thin film in steps of 1 V up to 7 V, 5 s per step and measuring the tip displacement at each step with an AC signal of amplitude 2 V with a 1 s read time. Contrary to ferroelectric maps, in hysteresis loops, we took advantage of an effective amplification ( $Q_{\text{eff}} = 8.5$ ) obtained working at a frequency ( $f_{\text{meas}} \sim 288 \text{ kHz}$ ) in the vicinity of the contact resonance. The piezoelectric coefficient is evaluated as  $d_{33} = S \times A_{\text{PFM}} / (Q_{\text{eff}} \times G \times V_{\text{ac}})$ , where  $S$  indicates the tip sensitivity,  $A_{\text{PFM}}$  the maximum amplitude span in the stress butterfly loop,  $G$  the gain, and  $V_{\text{ac}}$  the applied reading voltage.<sup>21</sup> The tip sensitivity was measured during the tip approach (209 nm/V), while the overall gain of the amplifier,  $G$ , was 225. Conductive atomic force microscopy scans were performed to identify a possible relationship between morphological features, ferro-piezoelectric spontaneous domains, and local current conduction. Sample areas of  $1\text{--}5 \mu\text{m}^2$  were scanned at variable bias voltages in the 1–6 V range.

## III. RESULTS

### A. Conditions for epitaxial growth

To identify optimal conditions for epitaxial growth to achieve (001) oriented flat films without outgrowths, defects, or grain boundaries, 300 nm thick KNN samples were grown by PLD at a fixed oxygen pressure of 220 mTorr and target–substrate distance

of 40 mm while varying the substrate temperature in the range 470–740 °C. The surface morphology of six KNN thin film samples grown at 740, 660, 610, 560, 520, and 470 °C is displayed for comparison in Fig. 1. Cross-sectional SEM images are depicted in the corresponding insets. The sample grown at the highest temperature of 740 °C [Fig. 1(a)] shows a flat surface in the background with squared, pyramidal, and rod-shaped defect crystallites; the latter of 100–200 nm in size and several hundreds of nanometers (400–600 nm) in height, together with film cracks, aligned to the [100] or [010] directions of the Nb:STO substrate. Growth at 660 °C [Fig. 1(b)] leads to a remarkably smoother surface with only square-shaped oriented crystallites, always aligned to the [100] and [010] directions of the substrate with a height of a few tens of nanometers (20–40 nm). The number of crystallites increases when the growth temperature is reduced [see Fig. 1(c) for 610 °C] until the thermal budget is not enough to obtain a compact film [570 °C, Fig. 1(d)]. Grains and boundaries with voids in between are found for growth temperatures below 570 °C [Figs. 1(e)–1(f)]. The appearance of segregated crystallites of KNN onto STO has been attributed before to a significant lattice mismatch. When the mismatch is reduced, a more planar quality develops.<sup>22</sup>

From each sample, *in situ* RHEED reflections were collected after growth with a primary beam energy of 30 keV. An example is shown in Fig. 2, comparing electron diffraction patterns collected along the [100] direction of the substrate for all samples. Noteworthy, diffraction patterns taken on the substrate (not shown)

display almost the same stripe spacing, thus signaling a cube-on-cube growth of KNN on STO, as expected from a reduced lattice misfit of 1.1% between STO and KNN ( $a_{\text{STO}} = 3.905 \text{ \AA}$ <sup>23</sup> and  $a_{\text{KNN}} = 3.947$ ).<sup>22</sup> RHEED cannot readily appreciate such minor variations of the lattice constant; thus, they were investigated by XRD instead (see later in Sec. III D).

The RHEED signal of the sample grown at 740 °C, shown in Fig. 2(a), features some bright spots in the pattern. The appearance of spots is consistent with the sizable 3D features observed in the morphology of Fig. 1(a): the probing electron beam passes through these crystallites; therefore, a bulk-like transmission signal contribution is generated in the final diffraction pattern. A more distinctive RHEED striped pattern is mainly exhibited by samples deposited at 660 and 610 °C, compatible with a “2D-like” epitaxial growth of KNN on Nb:STO (001) [Figs. 2(b) and 2(c)]. However, the existence of outgrowths and crystallites still causes the appearance of spots inside the streaks due to electrons transmitted through those 3D structures. This is particularly observed for the film grown at 610 °C, which presents a significant amount of crystallites compared to the sample deposited at 660 °C. The bright spot structures clearly related to rough 3D growth modes reappear at lower growth temperatures below 570 °C [Figs. 2(d) and 2(e)]. The diffraction pattern is less distinct in the final sample at 470 °C, which suggests the formation of less organized crystal structures that might deviate from an effective epitaxial growth condition [Fig. 2(f)], as also evident in the SEM cross section [Fig. 1(f)].

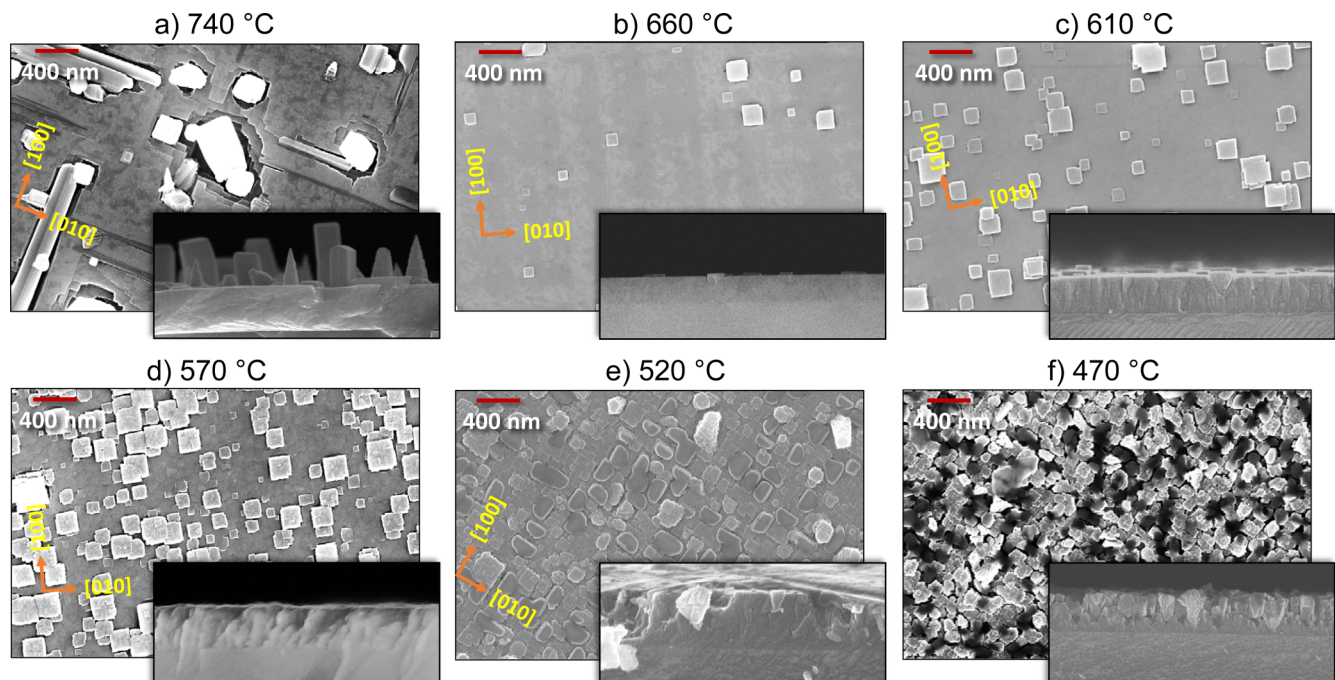


**FIG. 1.** SEM top view of the surface and cross section (insets) of KNN thin films deposited at different growth temperatures. Epitaxial crystalline ordering below 600 °C is not achieved, possibly due to the insufficient thermal budget that leads to increased roughness and worse compactness.

29 April 2024 13:07:06



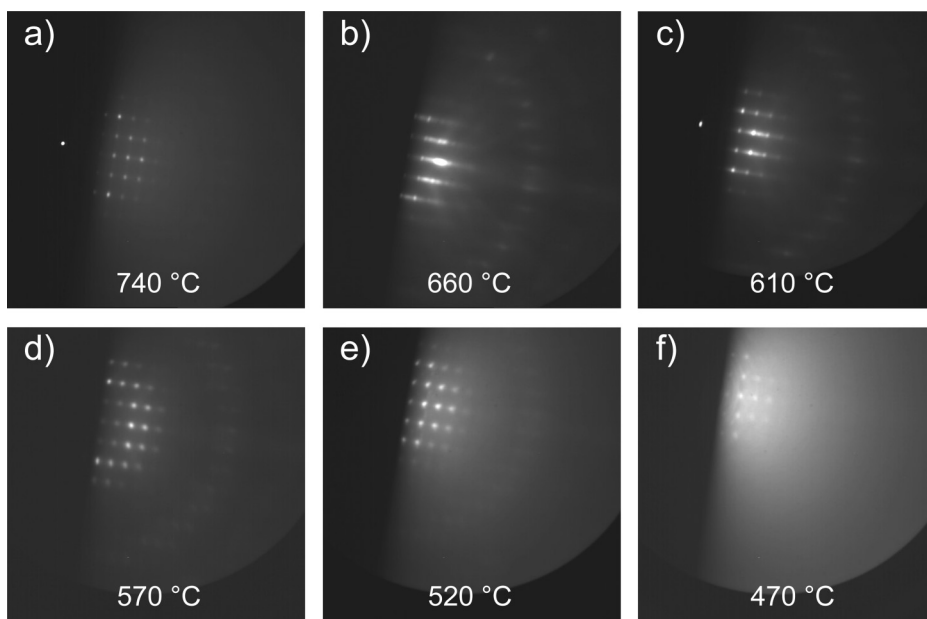


**FIG. 2.** RHEED diffraction patterns of the KNN thin films collected along the [100] in-plane direction of the Nb:STO substrate. Grazing incidence diffraction stripes and spots are displayed by 660 and 610 °C samples, suggesting a semi-2D-growth mode. In all other samples, transmission diffraction spots appear from roughness features generated by a clearly 3D island growth mode.

### B. Leakage caused by Na and K deficiency

The electrical performance of films grown at different temperatures was examined and compared by acquiring current–voltage ( $J$ – $V$ ) curves between adjacent electrodes (in a top-top configuration) as a function of the applied electric field, as reported in Fig. 3. Clearly, the leakage current is seen to monotonically increase with the temperature by almost eight orders of magnitude from 470 to 740 °C. This trend may appear at odds with the general belief that

defects, pinholes, and grain boundaries in porous, rough, fractured, and non-uniform surfaces significantly contribute to the current leakage. It suggests that intrinsic conduction mechanisms strictly associated with the deposition temperature may even dominate over morphological features so that rough 3D-like samples grown at 470 °C actually display the lowest leakage.

Chemical analysis using EDX (Fig. 4) may indicate the origin of these mechanisms. Indeed, we found that samples with lower

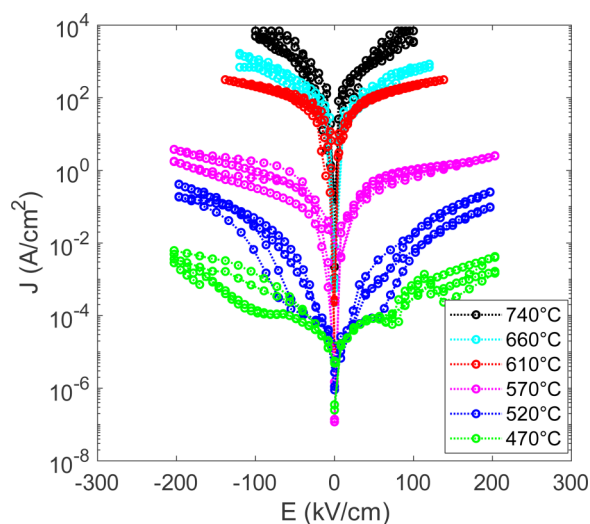


**FIG. 3.** Comparison of leakage current density curves for all KNN film samples grown from 740 to 470 °C. Lowering the growth temperature by 300 °C reduces leakage currents by almost eight orders of magnitude.

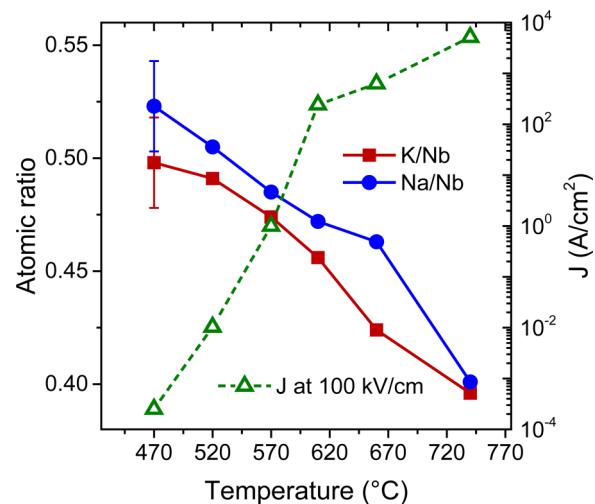
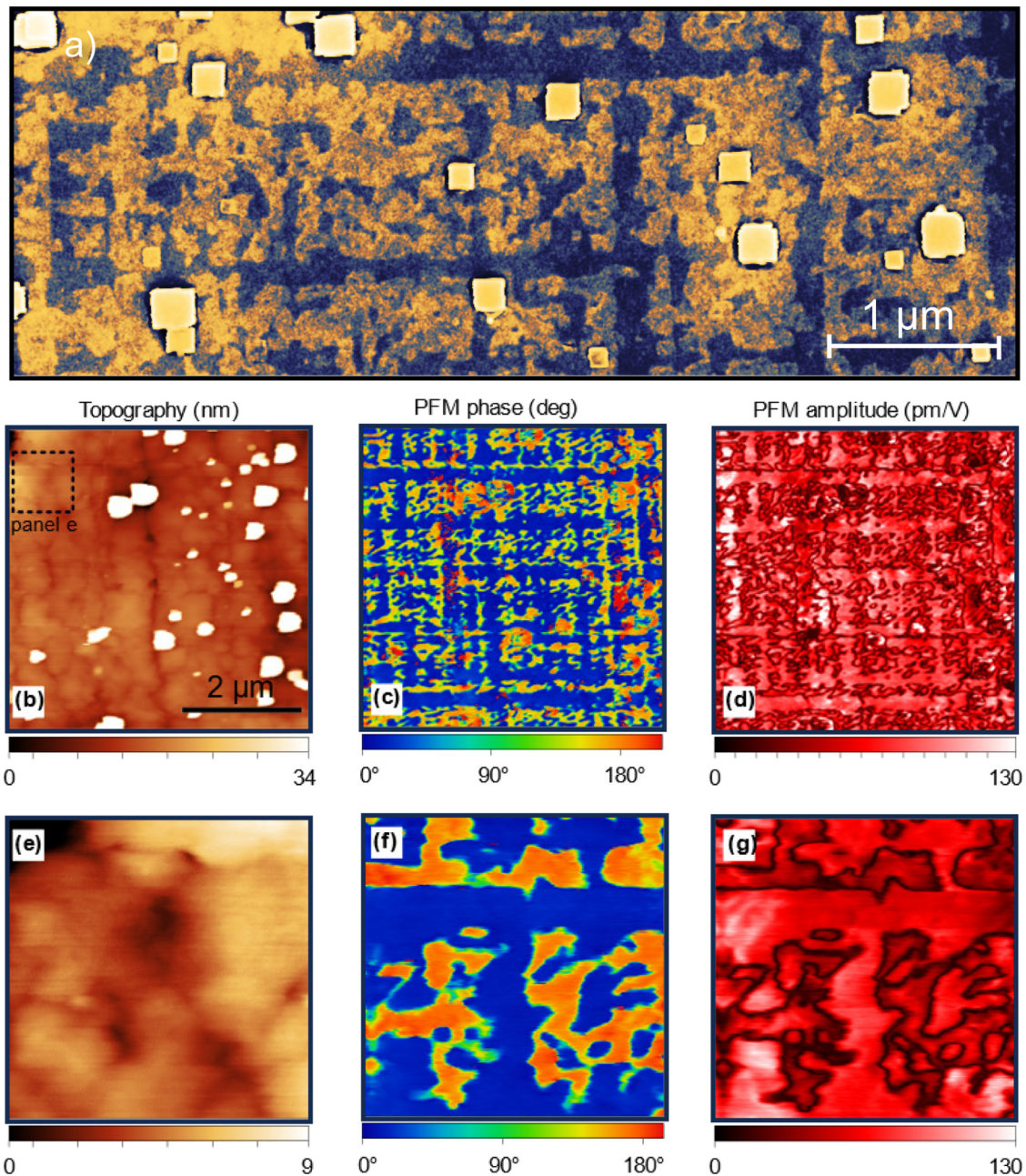


**FIG. 4.** Atomic ratios and leakage current density ( $J$ ) vs substrate growth temperature. High growth temperatures trigger the volatilization of alkali elements, and the resulting samples are, thus, under stoichiometric and leaky. In contrast, the atomic ratios of the samples deposited at lower temperatures are closer to the stoichiometric composition and generally more insulative.

29 April 2024 13:07:06

leakage currents grown at low temperatures have larger Na/Nb and K/Nb percentage ratios than those grown at higher temperatures. Flatter samples (grown at 610 and 660 °C) are notably under stoichiometric, whereas those deposited at temperatures below 600 °C

exhibit a chemical composition similar to the nominal one of the target, i.e.,  $K/Nb = 0.5$  and  $Na/Nb = 0.5$ . Volatilization of alkali (A) elements, in the form of  $A_2O$ , creates oxygen vacancies, which are super-oxidized, creating charge carriers.<sup>24–26</sup> Therefore, the growth



29 April 2024 13:07:06

**FIG. 5.** (a) SEM image of epitaxial KNN grown at 660 °C on STO. (b)–(d) Topography, the PFM phase, and PFM amplitude acquired by atomic force microscopy over a square of 5 μm. The PFM phase denotes the presence of opposite ferroelectric domains in the vertical direction (in blue and yellow), with the dominant polarization organized in horizontal and vertical stripes. The PFM amplitude is maximum within ferroelectric domains and reaches zero at the boundaries between them. (e)–(g) Topography, the PFM phase, and amplitude collected on a smaller region indicated by the dashed square of 1.2 μm sketched on panel (b).

temperature considerably influences how they are incorporated into the lattice and how they can be lost during deposition and subsequent annealing processes.<sup>27,28</sup> Due to the lack of alkali atoms at the A-sites, many intrinsic charged lattice vacancies are created in the  $\text{ABO}_3$  perovskite matrix. These vacancies can readily serve as hopping sites for charge transport, causing enhanced charge mobility through the thin film and deteriorating the insulating properties of the film.<sup>17,18</sup>

### C. Arrangement of ferroelectric domains of epitaxial KNN on Nb:STO

Backscattered electrons are sensitive to ferroelectric polarization as they are sensitive to charge accumulation effects and/or pyroelectric phenomena.<sup>29</sup> SEM characterization with the in-lens detector for backscattered electrons allowed us first to visualize orthogonal patterns in KNN epitaxial samples grown at 660 °C. This is evident in Fig. 5(a) after contrast enhancement using Gwyddion by means of an adaptative bimodal color filter.<sup>30</sup> Such a contrast was not observed for a growth temperature of 610 °C despite having fewer crystallites [Fig. 1(c) compared to Fig. 1(a) in grayscale]. To provide some insight into the pristine ferroelectric domain landscape, PFM and C-AFM measurements were carried out.

For the sample grown at 660 °C, Fig. 5 shows the typical topography [panels (b) and (e)], PFM phase [panels (c) and (f)], and amplitude [panels (d) and (g)] acquired by atomic force microscopy over 5 and 1.2  $\mu\text{m}$ , respectively. The piezoelectric response was obtained by applying an AC bias to the conductive tip of the AFM and recording the amplitude and the phase shift of the vertical oscillation of the cantilever induced by the piezoelectric displacement of the film with respect to voltage excitation. The excitation frequency (30 kHz) was much smaller than the contact resonance of the tip (330 kHz) to avoid any crosstalk between morphology and piezoelectric response. Spontaneous ferroelectric domains can be detected with inward and outward polarizations, as from RHEED patterns the films are known to be (001)-oriented. The phase map of panel Fig. 5(c) clearly shows the presence of out-of-plane ferroelectric polarization with two opposite orientations (with a phase difference of about 180° for blue and yellow regions). Overall, there is a net predominance of one orientation with respect to the other (75% vs 25% of the area in the panel) so that the pristine KNN film is polarized. The dominant ferroelectric polarization is organized in elongated horizontal and vertical stripes aligned to the cubic cell of the Nb:STO substrate. Such a ferroelectric landscape is supported by the map of the PFM amplitude [panel (d) in Fig. 5] representing an estimation of the piezoelectric coefficient  $d_{33}$ , which has barely similar values (20–100 pm/V) for inward and outward domains and approaches zero at the domain boundaries, as expected. The same information was also acquired on the smaller area represented by the dashed square in panel (b) (1.2  $\mu\text{m}$  side). On such a scale, it is possible to appreciate that local morphology (the presence of valleys about 3–4 nm deep, for example) is not directly correlated to the ferroelectric landscape [Fig. 5(f)]. Moreover, it is possible to clearly see the presence of domain boundaries with zero response in amplitude, as well as the stripes domains in the PFM phase.

To summarize, the ferroelectric film shows a pristine net polarization, with a ferroelectric landscape composed of horizontal and vertical stripes aligned to the [100] and [010] substrate directions and crossing each other perpendicularly. Such a structure is uncorrelated to the morphology of the film. Thus, we argue that such stripes might have originated from the interaction with the substrate, possibly providing an additional route for lattice strain relaxation.<sup>19,20,31,32</sup>

From the PFM amplitude signal, an evaluation of the  $d_{33}$  coefficient over the PFM amplitude map [Fig. 5(d)] of spontaneous domains can be obtained.<sup>21</sup> Over the area of  $5 \times 5 \mu\text{m}^2$ ,  $d_{33}$  spans from 20 to above 130 pm/V, the mean value is about 65 pm/V, and the standard deviation of the distribution is 30 pm/V. However, the mean value of the  $d_{33}$  coefficient is lower than that obtained from polycrystalline KNN films on Pt.<sup>15</sup> This could be partially attributed to some residual effects of substrate clamping,<sup>33,34</sup> while the primary reason for such reduction is probably related to the losses of Na and K that alter the film stoichiometry and interfere with effective voltage across the film.<sup>35</sup>

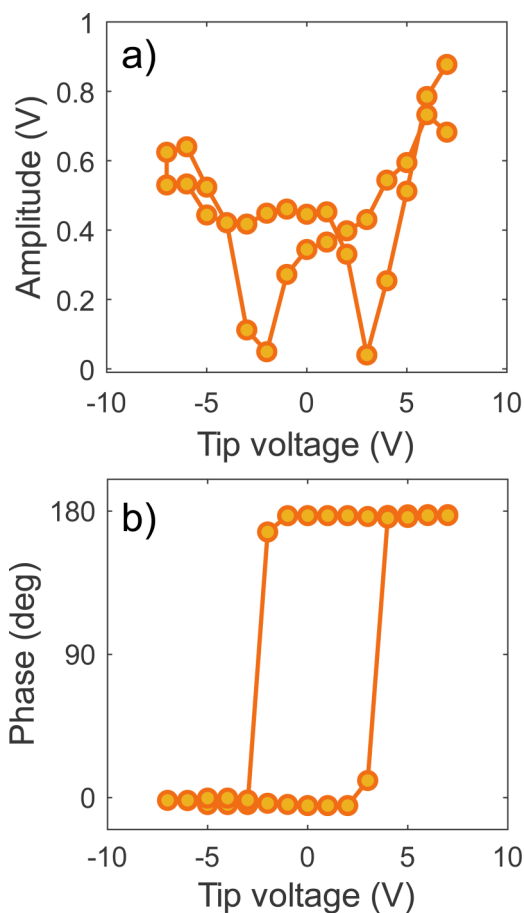


FIG. 6. Local piezoelectric amplitude (a) and phase (b) hysteresis loops of the 2D epitaxial sample grown at 660 °C.

29 April 2024 13:07:06



The analysis of local PFM switching hysteresis loops involves applying DC voltage pulses with increasing amplitude and superimposing an AC signal to detect the deflection at each DC bias. In this way, the displacement response at each bias is recorded and a complete loop can be plotted.<sup>36</sup> To generate the piezoelectric switching hysteresis loops seen in Fig. 6, the epitaxial sample grown at 660 °C was subjected to DC bias in increments of 1 V up to a maximum of 7 V. Exemplarily, Fig. 6 shows the hysteresis loop for the amplitude and phase of the piezoelectric signal. The semi-quantitative estimate for the piezoelectric coefficient on a specific point was 20 pm/V, thus within the range of values obtained from the imaging of spontaneous domains.

Interestingly, doing conductive atomic force microscopy scans of the vertical current across the thin film revealed evidence of the same horizontal and vertical patterns, imaged by the collected current. This can be seen in both the  $5 \times 5 \mu\text{m}^2$  area scanned at +5 V (applying the bias to the back side of the sample and keeping the tip

grounded) and the zoomed-in  $2 \times 2 \mu\text{m}^2$  area at +2 V in Figs. 7(b) and 7(d), respectively. The corresponding topography is provided in Figs. 7(a) and 7(c). The current signal reproduces the spontaneous domain pattern quite precisely with opposite out-of-plane polarizations of Fig. 5(b), with no significant correlation with the topography. A sizable current signal is collected from the domains with polarization opposite to the fixed bias field applied during the scan. In contrast, a smaller signal arises from domains parallel to the bias field where current is essentially given by leakage. We do not see a clear difference for opposite bias, but this is due to the asymmetry of the  $I(V)$  curve, as detailed below.<sup>35</sup> In general, the current signal acquired from consecutive scans was found to be quite reproducible, indicating that the depolarizing ferroelectric relaxation occurs over a time scale ranging from fractions of a second up to a few minutes required to complete a single scan before starting a new one.

Local  $I(V)$  current loops were acquired on a spot to corroborate our interpretation. A typical  $I(V)$  curve is shown in Fig. 7(e),

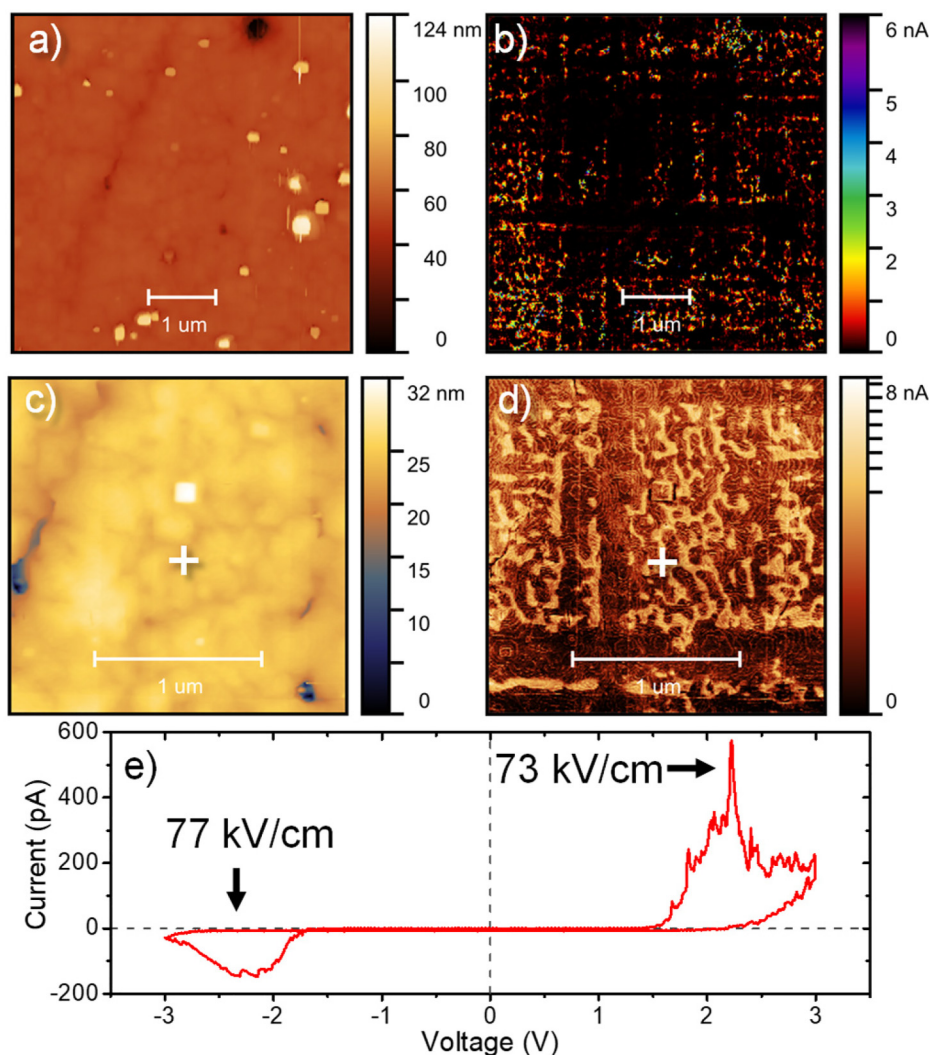


**FIG. 7.** C-AFM scans of the 660 °C sample with (a) and (c) topography and (b) and (d) current signal collected with a bias of 5 V on areas of  $5 \times 5$  and  $2 \times 2 \mu\text{m}^2$ , respectively. The squared configuration of the domains can clearly be imaged by the domain switching current signal. (e)  $I(V)$  loop measured at the cross position in the topography in (c) and (d).

29 April 2024 13:07:06



taken at the place marked by white crosses in the topographic picture of Figs. 7(c) and 7(d). Looking at the obtained typical  $I(V)$  curve presented in Fig. 7(e), it clearly exhibits the distinctive profile predicted for a ferroelectric material. Positive and negative current peaks are shown at about  $\pm 3$  V, corresponding to the ferroelectric coercive voltage observed in PFM loops in Fig. 5. However, the negative current amplitude and associated peak are lower, pointing to the presence of an asymmetric conduction mechanism in the tip/KNN/Nb:STO heterostructure system in analogy to what is discussed in a previous paper of ours.<sup>35</sup> This asymmetry can explain why the domain-related patterns are less evident for negative tip biases.

#### D. Epitaxial growth of KNN on the Nb:STO substrate

XRD data were collected from all samples to correlate the observed periodic domain pattern to lattice structure and strain deformations. Figure 8 shows symmetric, out-of-plane,  $\theta$ - $2\theta$  line scans of the samples, demonstrating an excellent epitaxial orientation of KNN, growing with a pseudo-cubic (001/100) orientation on cubic Nb:STO (001). It is remarkable, however, that films deposited at lower temperatures (570, 520, and 470 °C) display a prominent (100) orientation due to  $a$ -domains with the major axis of the tetragon in-plane, but yet with some evidence of the (001) orientation due to the presence of some  $c$ -domains (major axis out-of-plane). For samples deposited at higher temperatures (740, 660, and 610 °C), the orientation suddenly changes to (001), corresponding to domains with out-of-plane ferroelectric polarization. These assumptions were corroborated by in-plane XRD measurements, which clearly evidence a gradual compression effect of Nb:STO on KNN in an in-plane direction, thus promoting an

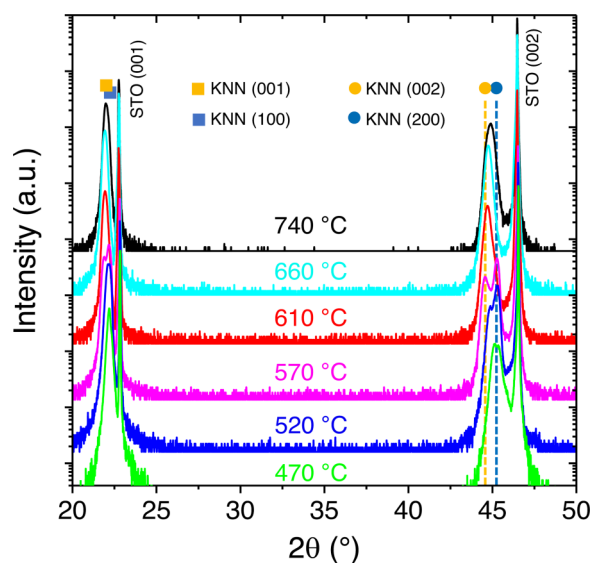
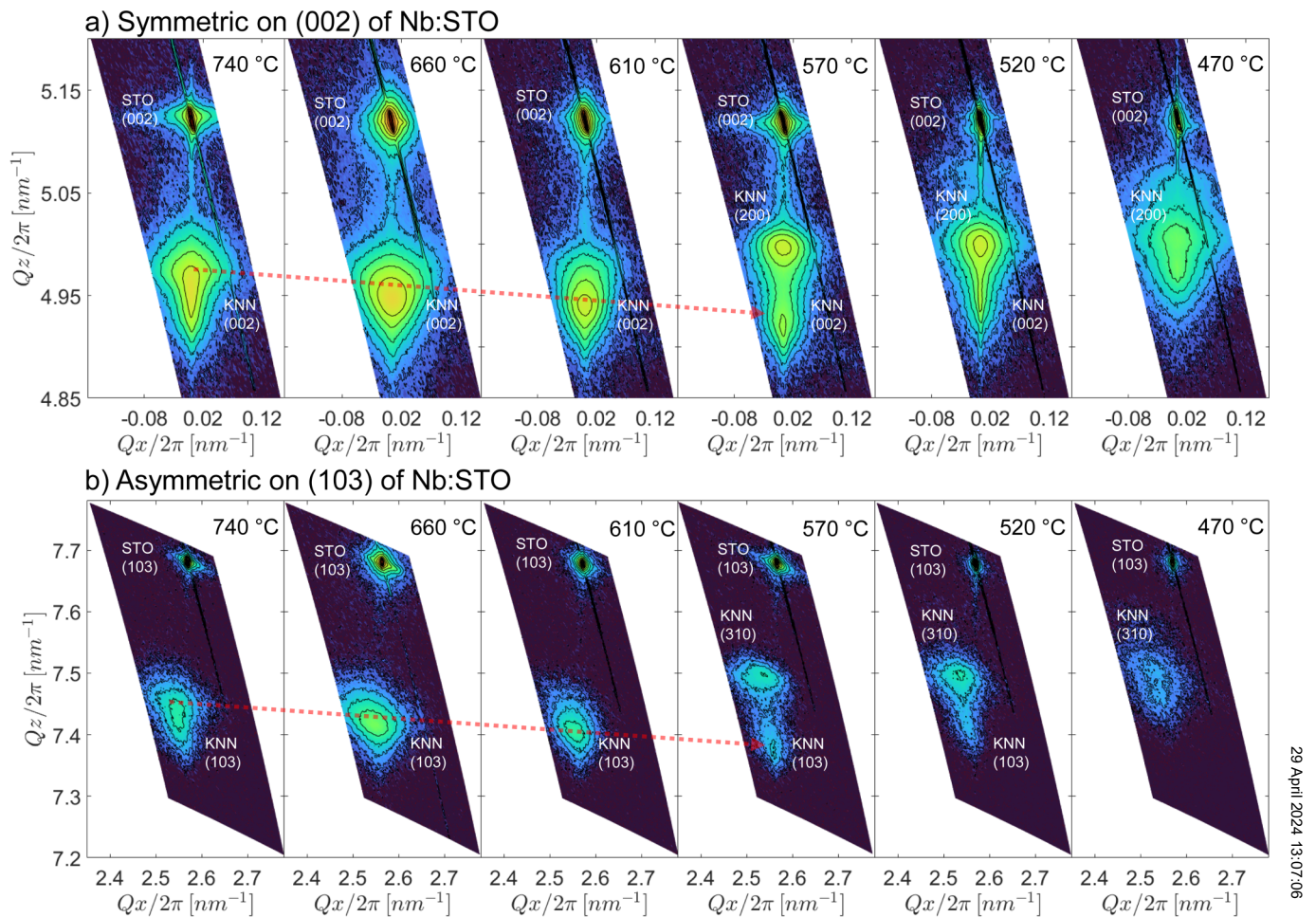


**FIG. 8.** Comparison of crystalline lattice reflections obtained from symmetric  $\theta$ - $2\theta$  out-of-plane XRD measurements of epitaxial KNN films grown on Nb:STO at various temperatures.

out-of-plane expansion. Such results are included and briefly discussed (Fig. S1 in the supplementary material).

To have a broader picture of how the KNN films adjust to the Nb:STO substrate according to the temperature of growth, reciprocal space mapping (RSM) measurements were performed. The RSM technique allows us to understand how the substrate and film's atomic planes might be related to each other. Such is achieved by selecting a known XRD reflection around a plane that is common to both materials and that allows to resolve them together. Then, range-limited  $\theta$ - $2\theta$  measurements are made recursively at various chosen  $\omega$  angles, which are inclinations around the normal of a chosen reflection, which might (symmetric) or might not (asymmetric) coincide with the sample surface's normal. In this way, a 2D map is produced by scanning vertical ( $\theta$ - $2\theta$ ) lines on  $\omega$  spacing, which can then be transformed into reciprocal space coordinates, thus the name of RSM.<sup>37</sup> In Fig. 9(a), reciprocal space maps of samples grown at various temperatures are compared and collected symmetrically (out-of-plane) around STO's (002) lattice reflection. As evidenced from  $\theta$ - $2\theta$  measurements and corroborated from the  $Q_x$  alignment of KNN and STO peaks in Fig. 9(a), the (002) and (200) planes of KNN are parallel to the (002)-plane of Nb:STO. Being an epitaxial substrate, Nb:STO appears as a spot with high intensity and limited dispersion. On the other hand, even though KNN is oriented with respect to Nb:STO, it displays a more significant dispersion (note that RSM figures are displayed in a logarithmic scale for intensity). Such observation indicates that KNN is of good crystal quality but also presents defects such as dislocations and stacking faults. The symmetric RSM of Fig. 9(a) allows us to see more clearly that a (200) orientation for KNN ( $a$ -domains) is dominant at low growth temperatures (around 570 °C and lower). However, a clear predominance of  $c$ -domains corresponding to the (002) orientation is seen for higher temperatures. A complete transition from (200) to (002) orientation is achieved at some intermediate temperatures between 570 and 610 °C. Interestingly, the lowest position in  $Q_z$  for the KNN (002) spot occurs at 570 °C, meaning the film is highly compressed (maximum elongation of the out-of-plane  $c$ -axis). Above that temperature, the value of  $c$  for KNN decreases with increasing temperature (position of the spot increases in  $Q_z$ ), and the shape of the KNN (002) spot becomes less symmetric. This points to a structural relaxation (decrease of strain) of the KNN crystalline cell. Interestingly, the sample grown at 740 °C displays a "tailed"  $Q_z$  distribution, meaning that, while most crystals decrease their  $c$ -lattice parameter, some retain the same value (arguably those closest to the KNN-Nb:STO interface). For a more complete picture, RSM was also made asymmetrically around the (103)-plane of Nb:STO. In Fig. 9(b), (103) of the Nb:STO substrate is observed as the brightest spot, while the less intense and more dispersed ones belong to (103) and (310) of KNN. It is found that the spots are not fully aligned in  $Q_x$ . This is expected for pseudo-cubic or tetragonally oriented KNN structures on Nb:STO, which, due to different  $a$ - and  $c$ -parameters, do not align perfectly parallel to one another. Once again, RSM measurements, this time asymmetric, confirm the change from (100) to (001) out-of-plane orientation of KNN as the deposition temperature is increased. The predominance of a high- $Q_z$  KNN (310) spot for growth temperatures at and below 570 °C is evidence of shorter interplanar spacing due to a

29 April 2024 13:07:06



29 April 2024 13:07:06

**FIG. 9.** Reciprocal space maps of the KNN films grown on Nb:STO (a) symmetrically around (002) of KNN/STO, and (b) asymmetrically around (103) of pseudo-cubic KNN/STO.

preferential (100) orientation of KNN. As the growth temperature increases from 570 to 740 °C, the (103) spot of KNN becomes prevalent, signaling a complete change to the (001) orientation. Moreover, the interplanar distance of the (103) spot of KNN is maximum at 570 °C (maximum strain for KNN), but it gets lower at higher temperatures (relaxation process). Interestingly, as also noted for the symmetrical RSM of (002) KNN grown at 740 °C,  $Q_z$  is tailed for the (103) plane of KNN. Yet again, this indicates a distribution of interplanar distances, both out-of-plane and in-plane.

Our comprehensive 3D structural analysis allowed us to establish that our KNN films are epitaxial and follow a pseudo-cubic or tetragonal crystal ordering. From the out-of-plane, in-plane, and RSM measurements, we calculated  $a$ - and  $c$ -lattice parameters. The lattice parameters and cell volumes are summarized in Table I. Remarkably, the lattice spacing for KNN grown at 470 °C reproduces the reported values displayed by a pseudo-tetragonal, relaxed KNN ceramic (referred to as “bulk KNN”).<sup>22</sup> For all higher

deposition temperatures, the  $c$ -parameter is larger than for bulk KNN, while the  $a$ -parameter is smaller. For Nb:STO  $a = 3.9065$  Å, which indicates in-plane compressive strain for KNN with a corresponding stretched  $c$ -parameter out-of-plane when grown on Nb:

**TABLE I.** Lattice parameters and simple cell volume for bulk KNN and PLD-deposited KNN films on the Nb:STO substrate.

Temp. (°C)	$c$ (Å) out-of-plane	$a$ (Å) in-plane	$V$ (Å <sup>3</sup> )
740	4.036	3.927	62.251
660	4.043	3.938	62.711
610	4.050	3.938	62.793
570	4.059	3.943	63.096
520	4.035	3.947	62.872
470	4.015	3.955	62.815
Bulk KNN	4.016	3.947	62.564

STO.<sup>22</sup> Interestingly, while the  $a$ -parameter of KNN shows a marked reduction trend with raising temperature, its  $c$ -parameter presents a maximum at 570 °C. Such an effect is also reflected as the highest volume for the KNN cell at such temperature, thus indicating an elevated level of stress (Fig. S2 in the supplementary material). A relaxation of the volume and stress occurs above 570 °C, which is associated with the large loss of alkaline elements at high growth temperatures.<sup>32</sup>

#### IV. DISCUSSION

An explanation for the formation of an orthogonal domain configuration observed in flatter epitaxial samples on Nb:STO can lie in stress relaxation phenomena generated by the interplay of the elastic properties of the thin film and the substrate. There are two primary categories of stress relaxation mechanisms: the emergence of mixed ferroelectric domain structures and the creation of misfit dislocations.<sup>19</sup> Concerning the first type, some studies have shown that the areas near domain boundaries in epitaxial ferroelectric thin films operate to elastically accommodate strains brought on by lattice mismatch between the film and the substrate.<sup>38</sup> In this picture, if the release of the elastic energy of one monodomain is possible by introducing a second domain orientation, multiple domain formation is stimulated. Relaxing the epitaxial strain for  $c$ -domains gives rise to an orthogonal dislocation array with a single dislocation density.<sup>39</sup> On the other hand, the formation of misfit dislocations along the interface between the film and the substrate is a well-known stress release mechanism.

In light of what was discussed above, the simple cubic structure of the STO substrate ( $a = 3.905 \text{ \AA}$ ) is expected to exert a bi-axial compressive strain onto the KNN thin film (in the tetragonal bulk  $a_b = 3.947 \text{ \AA}$ ), as the lattice mismatch  $f = 100 \frac{a_{\text{STO}} - a_{\text{KNN},b}}{a_{\text{KNN},b}} = -1.06\%$ . As a matter of fact, the mismatch-induced deformation of KNN is reflected by a smaller and decreasing  $a$ -parameter, and a larger  $c$ -parameter in all film samples with respect to the tetragonal KNN bulk reference (Table I). Regarding the effect of the growth temperature, and despite the alkaline loss (Fig. 4), a volume maxima centered around 570 °C occurs when rising the growth temperature (Table I). At this point, a change of preferential (100) to (001) orientation out-of-plane occurs. According to XRD measurements, this is due to a larger compressive strain (in-plane stress) of the lattice cell, which can favor strain relaxation mechanisms connected to the formation of peculiar periodic domain patterns. A similar morphology and an associated domain pattern have been observed in similar works on the growth of perovskite oxides on SrTiO<sub>3</sub>. The surface morphology observed in our films is similar to what Saito *et al.* had previously reported in NaNbO<sub>3</sub> films on SrTiO<sub>3</sub> substrates.<sup>9</sup> This phenomenon is associated with surface undulations and ascribed to surface relieve patterns and ferroelastic domains.<sup>10,40</sup> They represent a secondary stress relief process that only occurs in thick films in addition to stress release through the creation of misfit dislocations.<sup>40</sup> The generation of this kind of surface morphology is suggested to be due to the interaction between greater surface energy and the release of strain energy by mass transport mechanisms activated during film slow deposition at high temperatures and/or during the post-growth final cooling step.<sup>9,10</sup>

Differences between piezoelectric coefficients measured on epitaxial KNN samples with respect to the results of KNN films grown on other substrates<sup>7,8</sup> have been shown to depend on misfit dislocations, which can cause deterioration of piezoelectric properties.<sup>41,42</sup> As a matter of fact, the ferroelectric polarization close to the dislocation regions can be suppressed by the strain field developed around the dislocation sites, which also creates a strongly confined polarization gradient.<sup>42</sup> On the other hand, pinning of the ferroelastic domain walls due to the strain coupling of ferroelastic domains and misfit dislocations may limit the mobility of the ferroelastic domain walls in an applied electric field and thereby decrease the extrinsic contribution to piezoelectric effects.<sup>42</sup> Notably, the structural properties of perovskite oxide thin films can be deliberately altered by suitably engineering the strain coupling of ferroelastic domains and misfit dislocations.

#### V. CONCLUSIONS

In this work, a detailed characterization of epitaxial KNN thin films grown by pulsed laser deposition on Nb:STO(001) as a function of substrate growth temperature was presented. At low temperatures, the films are 3D-grown, with poor morphology (470–570 °C) and a preferential (100) orientation with the  $c$ -axis out-of-plane for KNN. In the 610–660 °C window, they become flatter, (001)-oriented, and strongly epitaxial, while at 740 °C, a sizable density of crystallites with height up to 300 nm develops. The leakage current is almost independent of the film morphology while it strongly increases at high temperatures (by eight orders of magnitude) due to the high volatility of alkali atoms, which introduces vacancies and hopping sites for conduction. Interestingly enough, flat epitaxial films grown at 660 °C display a net spontaneous polarization, with the domains of the dominant (001)KNN orientation mainly organized in orthogonal stripes aligned to the [100]/[010] directions of the (001)Nb:STO substrate. We associate this phenomenon to a stress release mechanism through the accommodation of strain at piezoelectric domain walls that acts in parallel to the creation of misfit dislocations in highly alkali deficient films, which present large compressive strain and reduction of the cell volume for high deposition temperatures. These results indicate the possibility of exploiting thin film strain engineering to stabilize controlled ferroelectric and piezoelectric domain patterns.

#### SUPPLEMENTARY MATERIAL

In-plane x-ray diffraction measurements for the studied KNN films can be found in the supplementary material. A graph depicting the behavior of the lattice parameters of KNN has been included.

#### ACKNOWLEDGMENTS

The Joint Research Centre scientific partnership between Politecnico di Milano and STMicroelectronics supported this work. The authors acknowledge the availability of experimental facilities at PoliFAB.

29 April 2024, 13:07:06



## AUTHOR DECLARATIONS

## Conflict of Interest

R. Bertacco reports financial support from ST Microelectronics Inc. during the study.

## Author Contributions

**C. Groppi:** Conceptualization (equal); Data curation (equal); Formal analysis (equal); Investigation (lead); Methodology (lead); Writing – original draft (equal). **F. Maspero:** Data curation (equal); Formal analysis (equal); Supervision (lead); Writing – original draft (equal). **M. Asa:** Conceptualization (equal); Methodology (supporting); Supervision (lead); Writing – original draft (supporting). **G. Pavese:** Data curation (equal); Formal analysis (equal). **C. Rinaldi:** Data curation (equal); Formal analysis (lead); Methodology (equal). **E. Albisetti:** Data curation (equal); Investigation (equal); Resources (equal). **M. Badillo-Avila:** Data curation (lead); Formal analysis (equal); Methodology (lead); Validation (lead); Writing – original draft (lead). **R. Bertacco:** Conceptualization (lead); Formal analysis (lead); Funding acquisition (lead); Project administration (lead); Resources (lead); Supervision (lead); Validation (lead); Writing – original draft (equal).

## DATA AVAILABILITY

The data that support the findings of this study are available from the corresponding author upon reasonable request.

## REFERENCES

- <sup>1</sup>H. Kulkarni, K. Zohaib, A. Khusru, and K. Shravan Aiyappa, “Application of piezoelectric technology in automotive systems,” *Mater. Today Proc.* **5**(10), 21299–21304 (2018).
- <sup>2</sup>H. Elahi, K. Munir, M. Eugeni, M. Abrar, A. Khan, A. Arshad, and P. Gaudenzi, “A review on applications of piezoelectric materials in aerospace industry,” *Integr. Ferroelectr.* **211**(1), 25–44 (2020).
- <sup>3</sup>K. Xu, J. Li, X. Lv, J. Wu, X. Zhang, D. Xiao, and J. Zhu, “Superior piezoelectric properties in potassium-sodium niobate lead-free ceramics,” *Adv. Mater.* **28**(38), 8519–8523 (2016).
- <sup>4</sup>A. Safari and M. Abazari, “Lead-free piezoelectric ceramics and thin films,” *IEEE Trans. Ultrason. Ferroelectr. Freq. Control* **57**(10), 2165–2176 (2010).
- <sup>5</sup>Y. Saito, H. Takao, T. Tani, T. Nonoyama, K. Takatori, T. Homma, T. Nagaya, and M. Nakamura, “Lead-free piezoceramics,” *Nature* **432**(7013), 84–87 (2004).
- <sup>6</sup>J. Rödel, K. G. Webber, R. Dittmer, W. Jo, M. Kimura, and D. Damjanovic, “Transferring lead-free piezoelectric ceramics into application,” *J. Eur. Ceram. Soc.* **35**(6), 1659–1681 (2015).
- <sup>7</sup>M. D. Nguyen, M. Dekkers, E. P. Houwman, H. T. Vu, H. N. Vu, and G. Rijnders, “Lead-free (K<sub>0.5</sub>Na<sub>0.5</sub>)NbO<sub>3</sub> thin films by pulsed laser deposition driving MEMS-based piezoelectric cantilevers,” *Mater. Lett.* **164**, 413–416 (2016).
- <sup>8</sup>L.-S. Kang, B.-Y. Kim, I.-T. Seo, T.-G. Seong, J.-S. Kim, J.-W. Sun, D.-S. Paik, I. Hwang, B. H. Park, and S. Nahm, “Growth behavior and electrical properties of a (Na<sub>0.5</sub>K<sub>0.5</sub>)NbO<sub>3</sub> thin film deposited on a Pt/Ti/SiO<sub>2</sub>/Si substrate using RF magnetron sputtering,” *J. Am. Ceram. Soc.* **94**(7), 1970–1973 (2011).
- <sup>9</sup>T. Saito, H. Adachi, T. Wada, and H. Adachi, “Pulsed-laser deposition of ferroelectric NaNbO<sub>3</sub> thin films,” *Jpn. J. Appl. Phys.* **44**(9S), 6969 (2005).
- <sup>10</sup>M. Abazari Torghabeh, *Development of Lead-Free Piezoelectric Thin Films by Pulsed Laser Deposition* (The State University of New Jersey, 2010).

- <sup>11</sup>H. C. Thong, C. Zhao, Z. X. Zhu, X. Chen, J. F. Li, and K. Wang, “The impact of chemical heterogeneity in lead-free (K,Na)NbO<sub>3</sub> piezoelectric perovskite: Ferroelectric phase coexistence,” *Acta Mater.* **166**, 551–559 (2019).
- <sup>12</sup>A. Dahiya, O. P. Thakur, and J. K. Juneja, in *2013 Seventh International Conference on Sensing Technology* (IEEE, 2013), pp. 383–386.
- <sup>13</sup>Y. Tsujiura, E. Suwa, H. Hida, K. Suenaga, K. Shibata, and I. Kanno, in *2013 Transducers Eurosensors XXVII 17th International Conference on Solid-State Sensors, Actuators Microsystems (TRANSDUCERS EUROSENSORS XXVII)* (IEEE, 2013), pp. 474–477.
- <sup>14</sup>F. Xia, Y. Peng, S. Pala, R. Arakawa, W. Yue, P.-C. Tsao, C.-M. Chen, H. Liu, M. Teng, J. H. Park, and L. Lin, in *2023 IEEE 36th International Conference on Micro Electro Mechanical Systems* (IEEE, 2023), pp. 135–138.
- <sup>15</sup>C. Groppi, L. Mondonico, F. Maspero, C. Rinaldi, M. Asa, and R. Bertacco, “Effect of substrate preparation on the growth of lead-free piezoelectric (K<sub>0.5</sub>Na<sub>0.5</sub>)NbO<sub>3</sub> on Pt(111),” *J. Appl. Phys.* **129**(19), 194102 (2021).
- <sup>16</sup>J. Koruza, H. Liu, M. Höfling, M.-H. Zhang, and P. Veber, “(K,Na)NbO<sub>3</sub>-based piezoelectric single crystals: Growth methods, properties, and applications,” *J. Mater. Res.* **35**(8), 990–1016 (2020).
- <sup>17</sup>T. Tanaka, F. Oba, K. Tatsumi, M. Kunisu, M. Nakano, and H. Adachi, “Theoretical formation energy of oxygen-vacancies in oxides,” *Mater. Trans.* **43**(7), 1426–1429 (2002).
- <sup>18</sup>B. S. Kang, S. K. Choi, and C. H. Park, “Diffuse dielectric anomaly in perovskite-type ferroelectric oxides in the temperature range of 400–700 °C,” *J. Appl. Phys.* **94**(3), 1904–1911 (2003).
- <sup>19</sup>J. S. Speck and W. Pompe, “Domain configurations due to multiple misfit relaxation mechanisms in epitaxial ferroelectric thin films. I. Theory,” *J. Appl. Phys.* **76**(1), 466–476 (1994).
- <sup>20</sup>J. S. Speck, A. C. Daykin, A. Seifert, A. E. Romanov, and W. Pompe, “Domain configurations due to multiple misfit relaxation mechanisms in epitaxial ferroelectric thin films. III. Interfacial defects and domain misorientations,” *J. Appl. Phys.* **78**(3), 1696–1706 (1995).
- <sup>21</sup>E. Soergel, “Piezoresponse force microscopy (PFM),” *J. Phys. D: Appl. Phys.* **44**(46), 464003 (2011).
- <sup>22</sup>T. Saito, T. Wada, H. Adachi, and I. Kanno, “Pulsed laser deposition of high-quality (K,Na)NbO<sub>3</sub> thin films on SrTiO<sub>3</sub> substrate using high-density ceramic targets,” *Jpn. J. Appl. Phys.* **43**(9S), 6627 (2004).
- <sup>23</sup>A. Janotti, B. Jalan, S. Stemmer, and C. G. Van de Walle, “Effects of doping on the lattice parameter of SrTiO<sub>3</sub>,” *Appl. Phys. Lett.* **100**(26), 262104 (2012).
- <sup>24</sup>C. W. Ahn, S. Y. Lee, H. J. Lee, A. Ullah, J. S. Bae, E. D. Jeong, J. S. Choi, B. H. Park, and I. W. Kim, “The effect of K and Na excess on the ferroelectric and piezoelectric properties of K<sub>0.5</sub>Na<sub>0.5</sub>NbO<sub>3</sub> thin films,” *J. Phys. D: Appl. Phys.* **42**(21), 215304 (2009).
- <sup>25</sup>Y. Kizaki, Y. Noguchi, and M. Miyayama, “Defect control for low leakage current in K<sub>0.5</sub>Na<sub>0.5</sub>NbO<sub>3</sub> single crystals,” *Appl. Phys. Lett.* **89**(14), 142910 (2006).
- <sup>26</sup>M. A. Rafiq, M. E. Costa, A. Tkach, and P. M. Vilarinho, “Impedance analysis and conduction mechanisms of lead free potassium sodium niobate (KNN) single crystals and polycrystals: A comparison study,” *Cryst. Growth Des.* **15**(3), 1289–1294 (2015).
- <sup>27</sup>Y. Huan, X. Wang, T. Wei, J. Xie, Z. Ye, P. Zhao, and L. Li, “Defect engineering of high-performance potassium sodium niobate piezoelectric ceramics sintered in reducing atmosphere,” *J. Am. Ceram. Soc.* **100**(5), 2024–2033 (2017).
- <sup>28</sup>F. Hussain, I. Sterianou, A. Khesro, D. C. Sinclair, and I. M. Reaney, “p-type/n-type behaviour and functional properties of K<sub>x</sub>Na<sub>(1-x)</sub>NbO<sub>3</sub> (0.49 ≤ x ≤ 0.51) sintered in air and N<sub>2</sub>,” *J. Eur. Ceram. Soc.* **38**(9), 3118–3126 (2018).
- <sup>29</sup>S. Zhu and W. Cao, “Imaging of 180° ferroelectric domains in LiTaO<sub>3</sub> by means of scanning electron microscopy,” *Phys. Status Aolidi A* **173**(2), 495–502 (1999).
- <sup>30</sup>D. Nečas and P. Klapetek, “Gwyddion: An open-source software for SPM data analysis,” *Cent. Eur. J. Phys.* **10**(1), 181–188 (2012).
- <sup>31</sup>M. V. Rastei, F. Gellé, G. Schmerber, A. Quattropani, T. Fix, A. Dinia, A. Slaoui, and S. Colis, “Thickness dependence and strain effects in ferroelectric Bi<sub>2</sub>FeCrO<sub>6</sub> thin films,” *ACS Appl. Energy Mater.* **2**(12), 8550–8559 (2019).



- <sup>32</sup>M. Abazari, E. K. Akdoğan, and A. Safari, “Effects of background oxygen pressure on dielectric and ferroelectric properties of epitaxial  $(K_{0.44}Na_{0.52}Li_{0.04})(Nb_{0.84}Ta_{0.10}Sb_{0.06})O_3$  thin films on  $SrTiO_3$ ,” *Appl. Phys. Lett.* **93**(19), 192910 (2008).
- <sup>33</sup>N. Bassiri-Gharb, I. Fujii, E. Hong, S. Trolier-McKinstry, D. V. Taylor, and D. Damjanovic, “Domain wall contributions to the properties of piezoelectric thin films,” *J. Electroceram.* **19**(1), 49–67 (2007).
- <sup>34</sup>N. Ledermann, P. Murali, J. Baborowski, S. Gentil, K. Mukati, M. Cantoni, A. Seifert, and N. Setter, “{100}-textured, piezoelectric  $Pb(Zr_xTi_{1-x})O_3$  thin films for MEMS integration, deposition and properties,” *Sens. Actuators A* **105**(2), 162–170 (2003).
- <sup>35</sup>C. Groppi, F. Maspero, A. Rovelli, M. Asa, G. Malavena, C. M. Compagnoni, E. Albisetti, S. Vangelista, M. A. Badillo-Ávila, and R. Bertacco, “Electrode-dependent asymmetric conduction mechanisms in  $K_{0.5}Na_{0.5}NbO_3$  micro-capacitors,” *Mater. Sci. Semicond. Process.* **160**, 107422 (2023).
- <sup>36</sup>F. J. Flores-Ruiz, J. J. Gervacio-Arciniega, E. Murillo-Bracamontes, M. P. Cruz, J. M. Yáñez-Limón, and J. M. Siqueiros, “An alternative scheme to measure single-point hysteresis loops using piezoresponse force microscopy,” *Measurement* **108**, 143–151 (2017).
- <sup>37</sup>T. Konya, “X-ray thin-film measurement techniques III. High resolution x-ray diffractometry,” *Rigaku J.* **25**(2), 1 (2009).
- <sup>38</sup>W. Pompe, X. Gong, Z. Suo, and J. S. Speck, “Elastic energy release due to domain formation in the strained epitaxy of ferroelectric and ferroelastic films,” *J. Appl. Phys.* **74**(10), 6012–6019 (1993).
- <sup>39</sup>H. P. Sun, W. Tian, X. Q. Pan, J. H. Haeni, and D. G. Schlom, “Evolution of dislocation arrays in epitaxial  $BaTiO_3$  thin films grown on (100)  $SrTiO_3$ ,” *Appl. Phys. Lett.* **84**(17), 3298–3300 (2004).
- <sup>40</sup>W. K. Simon, E. K. Akdoğan, and A. Safari, “Anisotropic strain relaxation in  $(Ba_{0.6}Sr_{0.4})TiO_3$  epitaxial thin films,” *J. Appl. Phys.* **97**(10), 103530 (2005).
- <sup>41</sup>M.-W. Chu, I. Szafraniak, R. Scholz, C. Harnagea, D. Hesse, M. Alexe, and U. Gösele, “Impact of misfit dislocations on the polarization instability of epitaxial nanostructured ferroelectric perovskites,” *Nat. Mater.* **3**(2), 87–90 (2004).
- <sup>42</sup>V. Nagarajan, C. L. Jia, H. Kohlstedt, R. Waser, I. B. Misirlioglu, S. P. Alpay, and R. Ramesh, “Misfit dislocations in nanoscale ferroelectric heterostructures,” *Appl. Phys. Lett.* **86**(19), 192910 (2005).